Sensors and Materials, Vol. 34, No. 6 (2022) 2293–2309
MYU Tokyo

S & M 2973

Cavitation of Flow Field in Gear Pump

Jing-Nan Lin,[1] Yu-Ting Tseng,[1] Yan-Zuo Chang,[2*]
Yu-An Chou,[1] Go-Long Tsai,[1] and Tian-Syung Lan[3]

[1]The College of Mechanical & Electrical Engineering, National Taipei University of Technology, Taipei 106344, Taiwan ROC
[2]College of Mechatronic Engineering, Guangdong University of Petrochemical Technology, Maoming, Guangdong 525000, China
[3]Department of Information Management, Yu Da University of Science and Technology, Miaoli 361027, Taiwan ROC

(Received December 30, 2021; accepted April 13, 2022)

Keywords: gear pump, computational fluid dynamics, cavitation phenomenon

It is important to monitor the occurrence of cavitation in machines as it may damage them. Sensing technologies are used to monitor the occurrence of cavitation, but the mechanism of cavitation needs to be understood to implement appropriate sensing technologies at exact locations of machines. Therefore, a new simplified model was proposed and used with ANSYS Fluent to investigate how cavitation occurs in a gear pump. The model considers a transient state with a time step of as small as 2.5×10^{-6} s. In the model, the volume fraction and mixture properties were added to the continuity and momentum equations. Using the newly established model, a simulation was conducted to find the related parameters. Combinations of different numbers of modules and gear teeth were considered to observe the dynamic pressure distribution in the vicinity of gears to determine the locations of cavitation. The pressure was found to be high as 12.3 MPa in the oil-trapped area, and large pressure fluctuations of the outlet of the gear pump occurred when the oil-trapped pressure was released. The existence of cavitation during the operation of the gear pump was predicted by locating low-pressure areas. The amount of cavitation decreases when the flow rate of the pump increases with the increase in turbulence dynamic energy at saturated vapor pressure.

1. Introduction

There has been significant progress in the applications of fluid machines owing to new technologies, such as engine oil pumps, pressure devices in pipes, and jet engines. The reliability of machines has become an important issue in engineering when considering the cost and risk of wear. One of the factors affecting reliability is cavitation occurring during the operation of fluid-based machines, which reduces efficiency because it lowers the flow rate. It also gives rise to noise and shock waves, eventually resulting in severe damage to machines.

Cavitation appears when the fluid velocity undergoes a drastic change and the pressure drops to a value below the saturated vapor pressure because bubbles act similarly to those in the case

*Corresponding author: e-mail: changyanzuo@gmail.com
https://doi.org/10.18494/SAM3842

ISSN 0914-4935
https://myukk.org/

of boiling under this condition. These bubbles move to high-pressure zones and shrink until they burst. When a bubble bursts, a high flow velocity occurs, which results in a severe pressure shock and damage to solid surfaces. The pressure can be as high as 689 MPa.[1] A machine is thus damaged after the prolonged operation and pressure shocks due to bubble bursts.

In a pipe flow, cavitation has a similar effect to choking the flow of a compressible fluid because it blocks fluid transportation. Many analyses have been reported on this phenomenon. Sou *et al.* simulated the choke flow of a gasoline nozzle with the large eddy simulation (LES) turbulence model.[2] Lee *et al.* numerically studied the fuel nozzle of a supersonic scramjet at working temperature and pressure of 553 K and 1 MPa, respectively.[3] It was found that an increase in temperature induced a high saturated vapor pressure and caused more cavitation to occur.[4] Ramamurthy and Balachandar found that the noise and vibration reached the maximum level that the system can endure before the choke flow started to occur in a water tunnel.[5]

Inaguma employed a mathematical model to analyze the leakage of fluid from three types of gears: an external gear pump, an internal gear pump, and a vane pump.[6] According to the results, the working pressure, fluid temperature, rotating speed, and fluid characteristics affect the leakage and, in turn, reduce the volume efficiency. Močilana *et al.* established a 3D model for designing a gear pump with the Gambit commercial code, then analyzed the dynamic characteristics of the model with the finite volume method.[7] It was found that leakage was prevented by adjusting the contact of two gears.

Shen *et al.* analyzed the fatigue of a gear pump by using the ANSYS Fluent commercial code.[8] The maximal pressure was estimated and then employed to study the deformation and internal stress of the gears through solid mechanics. The solutions were imported into fatigue equations to obtain a probabilistic stress life curve (P-S-N curve).[9] The correlation between fatigue stresses and cycles was obtained. By using a 2D model with computational fluid dynamics (CFD), del Campo *et al.* found that cavitation occurred and that efficiency decreased when the rotation speed was increased.[10] Analyses with and without cavitation were conducted for comparison. In the numerical simulation with cavitation, the water hammer effect at the inlet was found to be the main reason for the reduced pumping efficiency. Singhal *et al.* presented a full cavitation model employing a simplified Rayleigh–Plesset equation.[11] The model considered the effects of surface tension and turbulent flow energy on saturated vapor pressure and non-condensable gases. On the basis of the model, the ACE+ commercial code was utilized to study the flow field around a hydrofoil, a cone, and an orifice. The simulation results were verified with experimental data. However, instability occurred in the simulation when many physical properties were considered together.[12]

To detect cavitation, several sensing technologies are necessary. Vibration, ultrasonic, pressure, and temperature sensors are mainly used for such a purpose. Monitoring the pressure, temperature, and vibration is critical for monitoring cavitation to prevent damage to machines. However, to use sensors correctly, it is necessary to understand how and where cavitation occurs. Therefore, we investigated cavitation in a gear pump by employing a numerical method with ANSYS Fluent. To validate the model's applicability, a simulation was also conducted. From the results, a condition that reduced the cavitation of the gear pump was found, providing basic information to improve the performance of gear pumps.

2. Methods

SolidWorks computer-aided design software was employed to model the gear pump and its surrounding area in this study. The model was then imported by ANSYS Workbench for the setting of the meshes, physical properties, and geometrical conditions.

2.1 Modeling

Figure 1 shows a schematic diagram of two gears and the upstream and downstream areas. The nodes of the two gears are in contact when they are in operation. In the simulation, a tiny gap between the two solid boundaries of the gears may cause difficulty in the meshing process and the severe skewness of the cells. Hence, the geometric design allowed gaps between the gears to avoid an auto combination problem. There were also slits between the gears and the shell. The gaps were wide enough to avoid instability and increase the calculation time in the computation.

The flow field was separated into three parts, namely, the inlet, gear, and outlet regions, which belong to a gear region that includes the vicinity of the gears and the gaps between the solid boundaries. In the inlet and outlet regions, structured (quadrilateral) cells were utilized with sparser meshing than that in the gear region. In the gear region, triangular cells and dense meshing were used owing to the marked velocity change in the gaps.

2.2 Parameter setup

The fluid was assumed to be a mixture of engine oil and steam. The density and viscosity of the engine oil were assumed to be 950 kg/m^3 and 0.019 Pa·s and those of steam were assumed to be 0.5542 kg/m^3 and 1.34 × 10^{-5} Pa·s, respectively. According to the Zwart–Gerber–Belamri (ZGB) cavitation model of corrosion and bubble dynamics, the diffusion velocity $\vec{V}_{dr,k}$ was

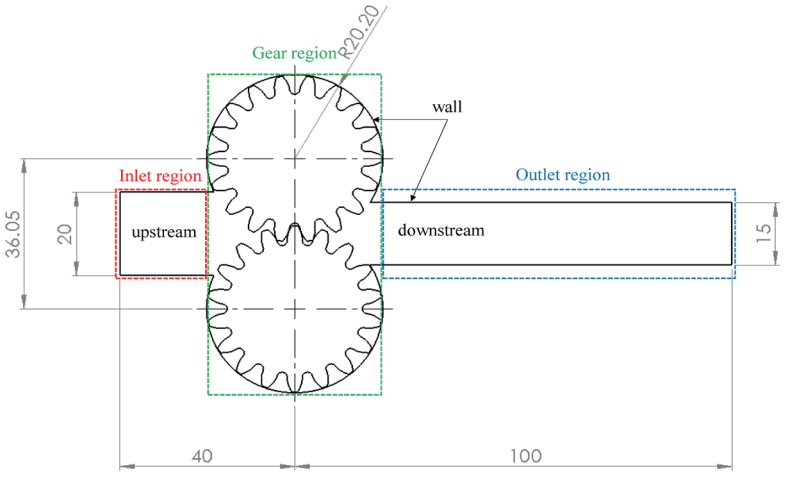

Fig. 1. (Color online) Schematic diagram of gears and flow field (lengths in mm).

ignorable. This simplified the simulation and reduced the computation time. In this study, the ZGB model was used for the cavitation model, for which the default parameters of a saturation pressure of 3540 Pa, a bubble radius of 10^{-6} m, a volume fraction of 0.0005, an evaporation coefficient of 50, and a condensation coefficient of 0.01 were set.[13]

The gear motion was set as rigid body motion in the dynamic meshing process. The rotation velocity was controlled by a user-defined function (UDF) but was set as constant in this study. The starting up time was ignored in the simulation[14] because the two gears were assumed to undergo rigid motion in the setting of the dynamic mesh, and the rotational speed was controlled by the UDF. Therefore, the rotational speed was set to a fixed value and the time for the motor to accelerate from zero to the working condition was ignored. Only the rotation speed of the gear was considered as a fixed value, so the unsteady behavior of the gear speed as it increased from zero to a fixed value was not considered.

The coupled pressure–velocity method was used for the parameter setup since its convergence was better than that of the semi-implicit method for the pressure-linked equations (SIMPLE) model.[15,16] The discretization method used was the least-squares cell-based gradient evaluation. PREssure STaggering Option (PRESTO) was used as the pressure interpolation method,[17] and the quadratic upwind interpolation of convective kinematics (QUICK) was used as the momentum volume integral method.[18]

Hybrid initialization was considered for the fast convergence of iterations.[19] The time step was 2.5×10^{-6} s based on the movement velocity and the remaining time of cavitation (20–30 μs).[20] There were 250 iterations in each time step, and the convergence criteria between two consecutive iterations were set with a relative deviation of less than 1×10^{3} for velocity and continuity.

The mesh file was imported into Fluent, and the detailed boundary conditions were assigned by the model. The numbers of modules and teeth were assumed to be 2 and 18, respectively. The width of the inlet was set to 20 mm, and the length from the inlet to the center was set to 40 mm. The corresponding width and length of the outlet were 15 and 100 mm, respectively. The pressures of the inlet and outlet were set as 1 and 6 bar, respectively. The saturated vapor pressure was 1.33 Pa. Gravity was ignored in the simulation.

Dense grids were assigned near the gears since the flow field was complicated and cavitation occurred in the region. The mesh in the inlet region was also refined to reduce the skewness of cells. The mass flow rate was estimated at the center of the inlet in the simulation. A mesh-independent test was performed to obtain a reliable result. The data obtained from the numerical analysis of various mesh designs are shown in Table 1. The average velocity of the inlet increased

Table 1
Various mesh designs (4000 time steps).

Total number of meshes	Number of triangle meshes	Number of quadrilateral meshes	Inlet velocity (m/s)	Elapsed time (h)
149500	132650	16850	9.27	4.5
257756	235306	22450	9.516	24
562104	528604	33500	9.797	11.5
922694	818069	104625	9.817	29.5
2379970	2111970	268000	9.898	48

with the grid number. However, the velocity saturated with increased mesh number, and a mesh number of 562104 was set to reduce the computing time.

2.3 Flow model

There are three methods in ANSYS/Fluent: Eulerian, Volume-of-fluid (VOF), and Mixture. The model with the Eulerian method was not used because of its time-consuming nature. The model with the VOF method was also not used because of the conflict of a basic assumption with cavitation. In the model with the Mixture method, the factor α_k is inserted in the continuity and momentum equations. This simplifies the complicated multiple-phase flow into a ratio relation. Thus, the equations are written as

$$\frac{\partial}{\partial t}\left(\rho_m\right)+\nabla\cdot\left(\rho_m\vec{V}_m\right)=0 \tag{1}$$

$$\frac{\partial}{\partial t}\left(\rho_m\vec{V}_m\right)+\rho_m\left(\vec{V}_m\cdot\nabla\right)\vec{V}_m=-\nabla P+\mu_m\nabla^2\vec{V}_m-\nabla\cdot\left(\sum_{k=1}^{n}\alpha_k\rho_k\vec{V}_{dr,k}\vec{V}_{dr,k}\right), \tag{2}$$

where $\vec{V}_m$ is the mass-averaged velocity, expressed as

$$\vec{V}_m=\frac{\sum_{k=1}^{n}\alpha_k\mu_k\vec{V}_k}{\rho_m}, \tag{3}$$

with α_k being the volume fraction of phase k.

The ratio relation is calculated as

$$\alpha_k=\frac{\forall_k}{\forall_{CV}}. \tag{4}$$

Therefore, $\alpha_k = 1$. That is, the control volume is entirely occupied by the fluid of phase k. The sum of all volume fractions is expressed as

$$\sum_{k=1}^{n}\alpha_k=1. \tag{5}$$

The mixture viscosity μ_m is written as

$$\mu_m=\sum_{k=1}^{n}\alpha_k\mu_k, \tag{6}$$

where ρ_m is the mixture density;

$$\rho_m = \sum_{k=1}^{n} \alpha_k \rho_k. \tag{7}$$

$\vec{V}_{dr,k}$ is the drift velocity between the primary and secondary phases, defined as

$$\vec{V}_{dr,k} = \vec{V}_k - \vec{V}_m. \tag{8}$$

The velocity $\vec{V}_{dr,k}$ is defined on the basis of the relative velocity $\vec{V}_{pq}$, where subscripts q and p are for the primary and secondary phases, respectively. Hence, $\vec{V}_{pq}$ is expressed as

$$\vec{V}_{pq} = \vec{V}_p - \vec{V}_q, \tag{9}$$

where c_k is the mass fraction of phase k and is defined as

$$c_k = \frac{\alpha_k \rho_k}{\rho_m}. \tag{10}$$

Therefore, the relationship between drift velocity and relative velocity is shown as

$$\vec{V}_{dr,k} = \vec{V}_{pq} - \sum_{k=1}^{n} c_k \vec{V}_{qk}. \tag{11}$$

The diffusion velocity results from the concentration difference between phases. However, cavitation occurred only in a short period; hence, the diffusion velocity is ignored in the simulation to simplify the process.

The continuity equation with the volume fraction is written as

$$\frac{\partial}{\partial t}\left(\alpha_p \rho_p\right) + \nabla \cdot \left(\alpha_p \rho_p \vec{V}_m\right) = -\nabla \cdot \left(\alpha_p \rho_p \vec{V}_{dr,p}\right) + \sum_{q=1}^{n} \left(\dot{m}_{pq} - \dot{m}_{qp}\right), \tag{12}$$

where $\dot{m}_{pq}$ is the rate of change of the transformation from phase p to phase q.
In the field of bubble dynamics,[21] the Rayleigh–Plesset equation is expressed as

$$\frac{P_B - P_\infty}{\rho_L} = R\frac{d^2R}{dt^2} + \frac{3}{2}\left(\frac{dR}{dt}\right)^2 + \frac{4\nu_L}{R}\frac{dR}{dt} + \frac{2\gamma}{\rho_L R}. \tag{13}$$

Ignoring the second-order terms, this equation is simplified to

$$\frac{dR}{dt} = \sqrt{\frac{2}{3}\frac{P_B - P_\infty}{\rho_L}}\,. \tag{14}$$

Because we use the ZGB model supplied by Fluent,[22] the cavitation model is based on the change in bubble mass (m_V). The rate of change in bubble mass is

$$\frac{dm_V}{dt} = \rho_V \frac{d\forall}{dt}, \tag{15}$$

where ρ_V is the bubble density and $\forall$ is the bubble volume. For a spherical bubble, $\forall = \frac{4}{3}\pi R^3$. Then, Eq. (15) is written as

$$\frac{dm_V}{dt} = \rho_V \frac{d}{dt}\left(\frac{4}{3}\pi R^3\right) = 4\pi R^2 \rho_V \frac{dR}{dt} = 4\pi R^2 \rho_V \sqrt{\frac{2}{3}\frac{P_B - P_\infty}{\rho_L}}\,. \tag{16}$$

The bubble volume fraction α_V as a function of the number of bubbles per unit volume is expressed as

$$\alpha_V = N_B \forall = N_B \frac{4}{3}\pi R^3, \tag{17}$$

The rate of change in mass due to cavitation is

$$\dot{S}_{lv} = \frac{3\alpha_V \rho_V}{R}\sqrt{\frac{2}{3}\frac{P_B - P_\infty}{\rho_L}}\,. \tag{18}$$

Considering the bubble size as a function of pressure, the rate of change in mass is rewritten as

$$\dot{S}_{lv} = F\frac{3\alpha_V \rho_V}{R}\sqrt{\frac{2}{3}\frac{\left|P_B - P_\infty\right|}{\rho_L}}\,, \tag{19}$$

where F is a correcting factor.

In addition, a new parameter, $\alpha_{nuc}\left(1-\alpha_V\right)$, was added to avoid instability due to the condensation of evaporated fluid.

$$\dot{S}_{lv} = \begin{cases} F_{vap}\dfrac{3\alpha_{nuc}\left(1-\alpha_V\right)\rho_V}{R}\sqrt{\dfrac{2}{3}\dfrac{P_V - P}{\rho_L}}, P_V > P \\ F_{cond}\dfrac{3\alpha_V \rho_V}{R}\sqrt{\dfrac{2}{3}\dfrac{P - P_V}{\rho_L}}, P > P_V \end{cases} \tag{20}$$

The parameters were as follows: evaporation coefficient $F_{vap} = 50$, condensing factor $F_{cond} = 0.01$, nucleation volume fraction $\alpha_{nuc} = 5 \times 10^{-4}$, and bubble radius $R = 10^{-6}$(m).

The aforementioned saturated vapor pressure P_{sat} is determined by turbulence.[23] The relation is expressed as

$$P_V = P_{sat} + \frac{1}{2}\left(0.39\rho_L k\right), \tag{21}$$

where k is the turbulent flow energy, i.e., the average of fluctuations in all directions, and is expressed as

$$k = \frac{1}{2}\left(\overline{u'u'} + \overline{v'v'} + \overline{w'w'}\right). \tag{22}$$

3. Results and Discussion

When gears rotate, the pressure of fluids fluctuates in the flow field due to engagement and separation. Figure 2 shows the monitoring points at the inlet and outlet used to investigate the pressure changes. Figures 3 and 4 show that the pressure changes periodically with the gear

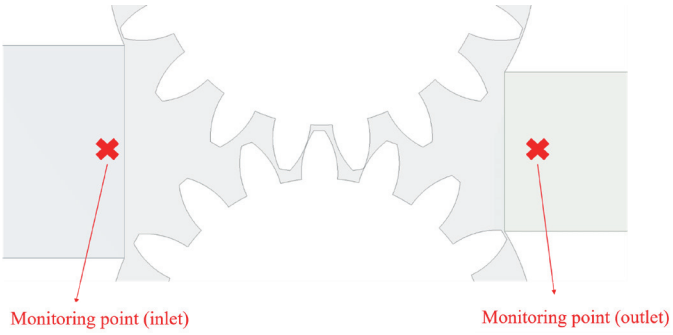

Fig. 2. (Color online) Locations of monitoring points.

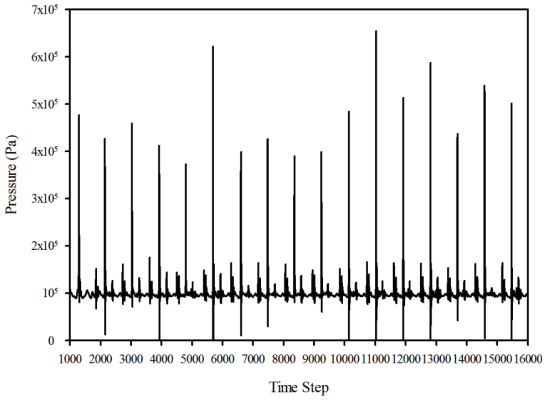

Fig. 3. Pressure fluctuations (monitoring point at the inlet, with leakage).

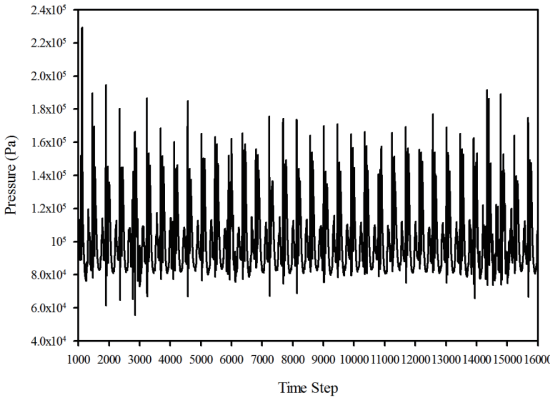

Fig. 4. Pressure fluctuations (monitoring point at the inlet, without leakage).

motion. The inlet pressure is sometimes close to the outlet pressure (Fig. 3). This is mainly attributed to the leakage problem. The numerical model did not perform gear engagement as in a real situation as explained in Refs. 24 and 25.

3.1 Pressure fluctuations

The proposed model was superior to the previous ones for analyzing the pressure fluctuations even though the pressure at the monitoring points was similar to that of the other models. In the case of leakage (Fig. 4), a fast Fourier transform (FFT) revealed that the pressure fluctuation frequency was close to the engagement frequency (900 Hz) (Fig. 5). Figure 6 shows a comparison between the numerical and experimental results.

As shown in Fig. 7, negative pressure occurred near the rotating zone of the gear, which is the flow field within the gear motion as shown in Fig. 1. Fluid was attracted into this area from the

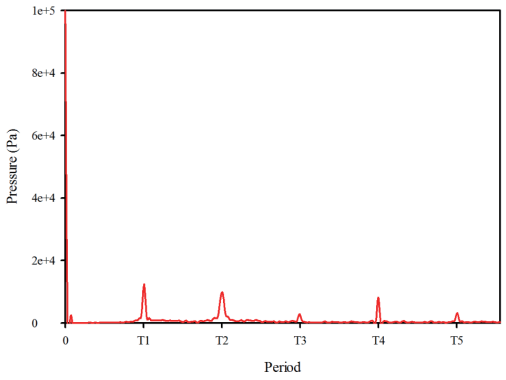

Fig. 5. (Color online) Pressure fluctuations obtained by FFT analysis.

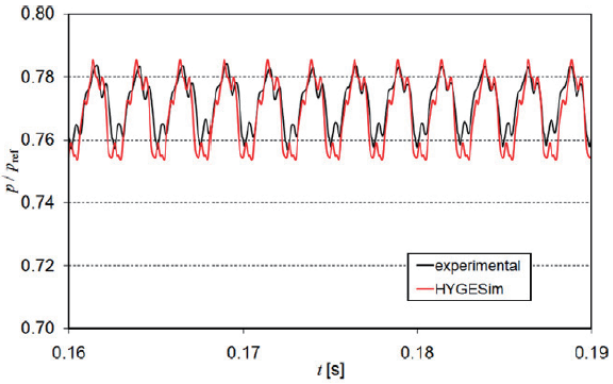

Fig. 6. (Color online) Pressure fluctuations at the outlet[26] in the experiment (black line) and simulation (red line).

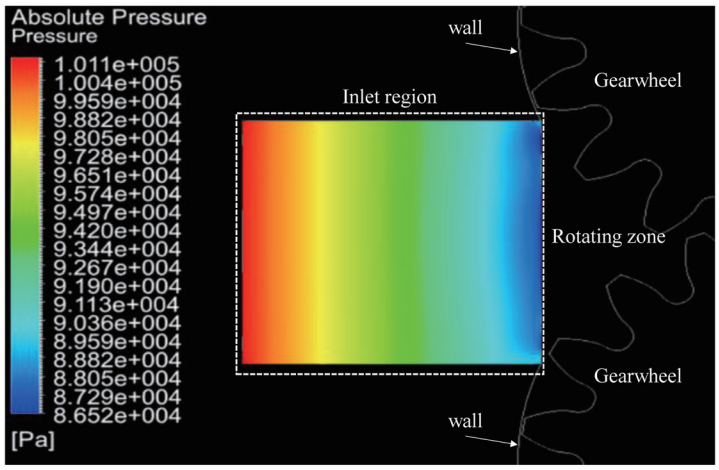

Fig. 7. (Color online) Pressure distribution at the inlet (absolute pressure).

inlet. Figure 8 presents the pressure distribution in the gear region. Cavitation occurs at locations where the pressure is less than the saturated vapor pressure. The pressure is as high as 12.3 MPa in the oil-trapped area, which is formed in a closed volume when a pair of gear teeth mesh at the same time. In the 2D model of this study, the trapped oil cannot flow to the outlet, so the area maintains the oil at high pressure.

Figure 9 shows the pressure distribution at the outlet. The flow moves and its pressure changes owing to gear rotation. High pressure accumulates in the oil-trapped area. When the pressure in this area is lowered, the outlet is subjected to high pressure. The consecutive variations in pressure result in a pressure wave at the outlet.

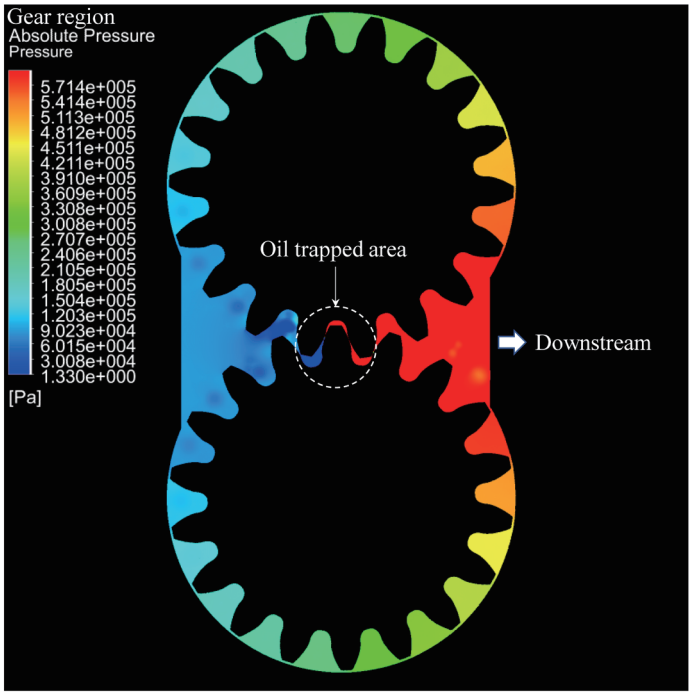

Fig. 8. (Color online) Pressure distribution in the gear rotation zone.

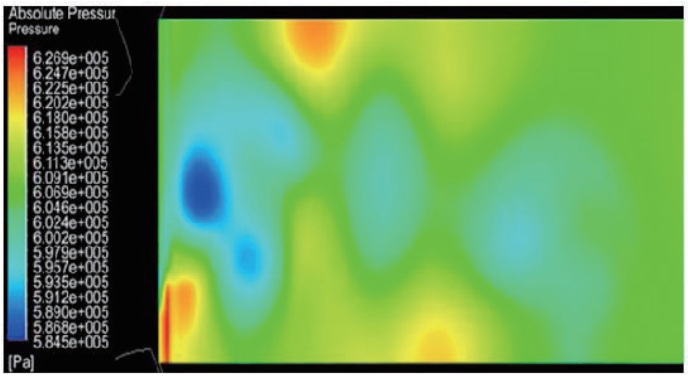

Fig. 9. (Color online) Pressure distribution at the outlet.

3.2 Verification of mass flow rate

The fluctuation of the inlet mass flow rate is similar to that of the pressure at the monitoring points. Moreover, the maximal flow rate occurred 2.5 × 10^{-5} s before the occurrence of the highest pressure. This suggests the leakage of oil in this model. Compared with the data of Ref. 27, the flow rate in this study exhibits a longer and larger fluctuation before convergence (Fig. 10).

Figure 11 shows the sinusoidal pattern of the flow rate with time, which is similar to the data in Refs. 28 and 29. As the reason for the sinusoidal pattern, the periodic appearance and extinction of the vacuum zone in the gear pump cause a pulsating flow pattern during operation.

Figure 12 shows the mass flow rate of the inlet with two modules and 18 gear teeth as a function of the number of time steps. Here, the module is a basic parameter of the gear teeth and is used to measure and determine the size of the gear teeth (module = pitch/π).

Figure 13 presents the results of the FFT analysis to obtain the flow rate. A peak appears at a frequency of 900 Hz. Figures 14 and 15 respectively present the flow rate and the FFT of the model with three modules and eight gear teeth. The frequency decreases to 400 Hz with the decreased number of gear teeth. On the other hand, the amplitude of the fluctuation increases with the increased number of modules.

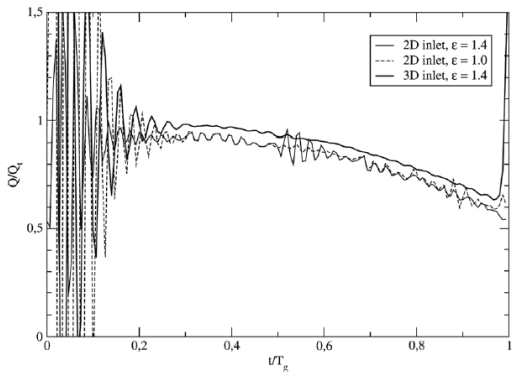

Fig. 10. Inlet mass flow rate with time.[29]

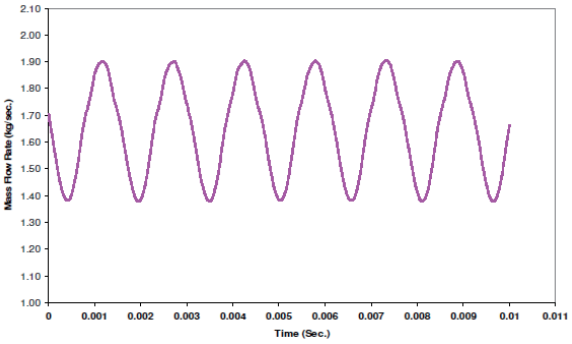

Fig. 11. (Color online) Mass flow rate with time.[30]

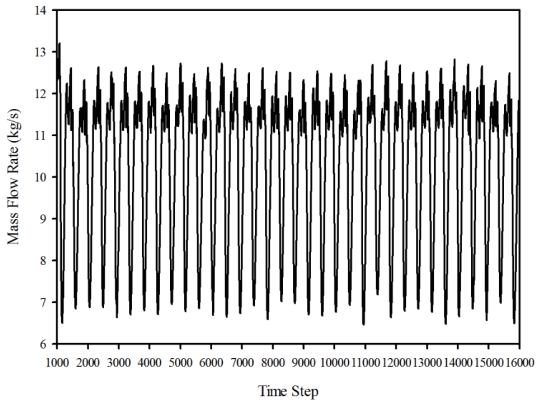

Fig. 12. Mass flow rate of inlet (modules = 2, teeth = 18).

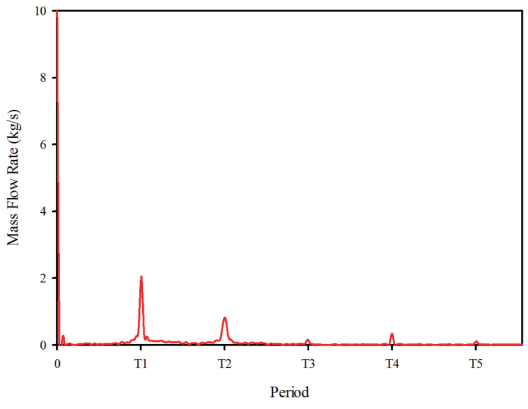

Fig. 13. (Color online) Mass flow rate of inlet obtained by FFT analysis (modules = 2, teeth = 18).

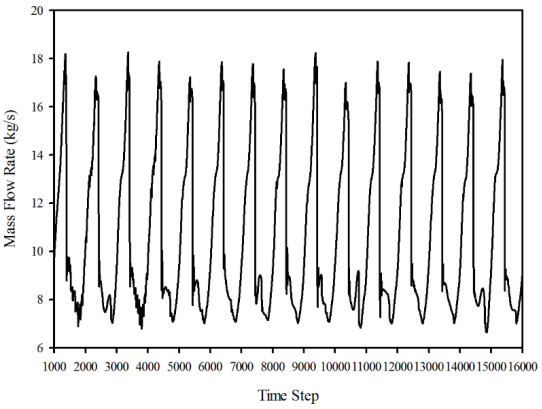

Fig. 14. Mass flow rate of inlet (modules = 3, teeth = 8).

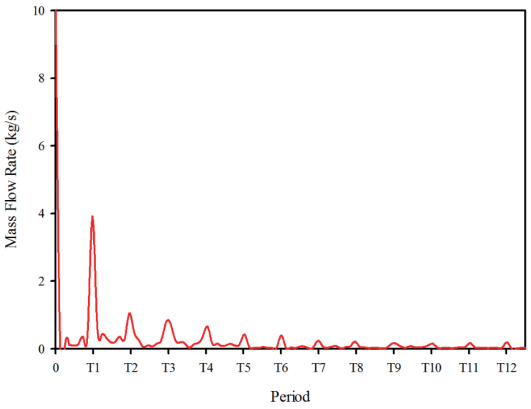

Fig. 15. (Color online) Mass flow rate of inlet obtained by FFT analysis (modules = 3, teeth = 8).

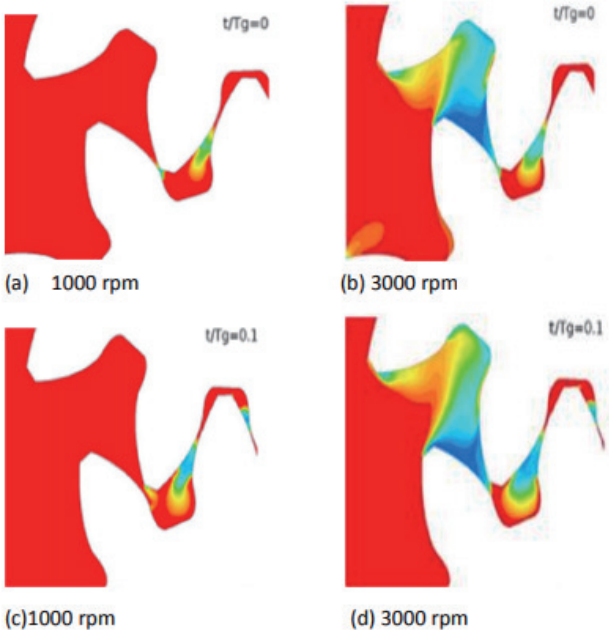

Fig. 16. (Color online) Effect of increasing speed on cavitation phenomenon.[31]

3.3 Cavitation locations

The locations of cavitation were verified using the results of other research. According to our simulation, cavitation occurs at engagement points as well as separation points. The locations of cavitation in this simulation are similar to those observed from high-speed photographs.[31]

Figure 16 shows that the cavitation becomes more severe when the rotating speed increases to 3000 rpm. Then, the pressure and flow rate at the monitoring point of the outlet are affected, and the flow changes from laminar to turbulent.[32] The results of the simulation of the flow change are shown in Fig. 17. The related data are also shown in Table 2. The VOF method simulates two or more immiscible fluids by solving a single momentum equation and tracking the volume

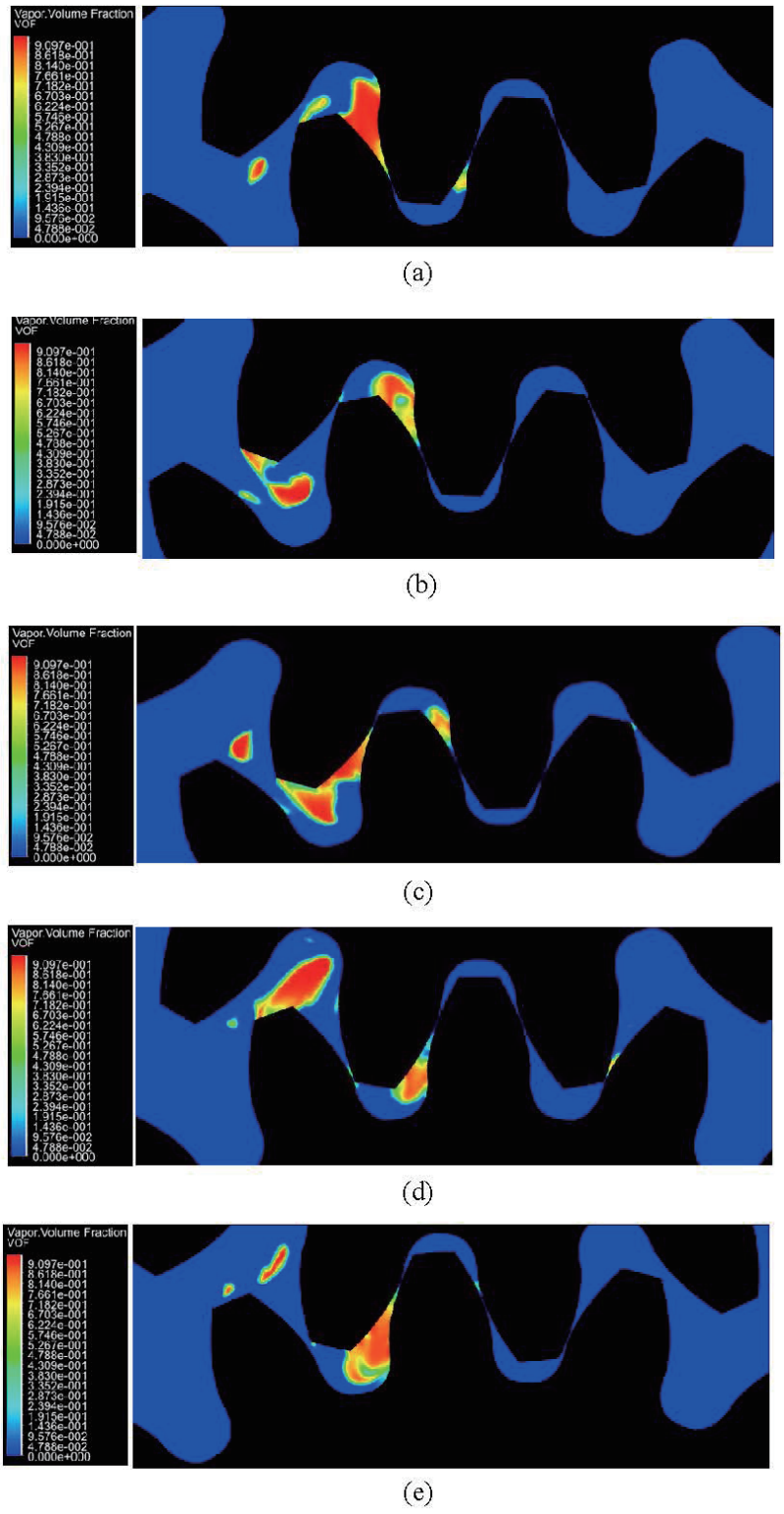

Fig. 17. (Color online) Vapor distributions at different times (s): (a) 0.004, (b) 0.008, (c) 0.012, (d) 0.016, and (e) 0.020 s.

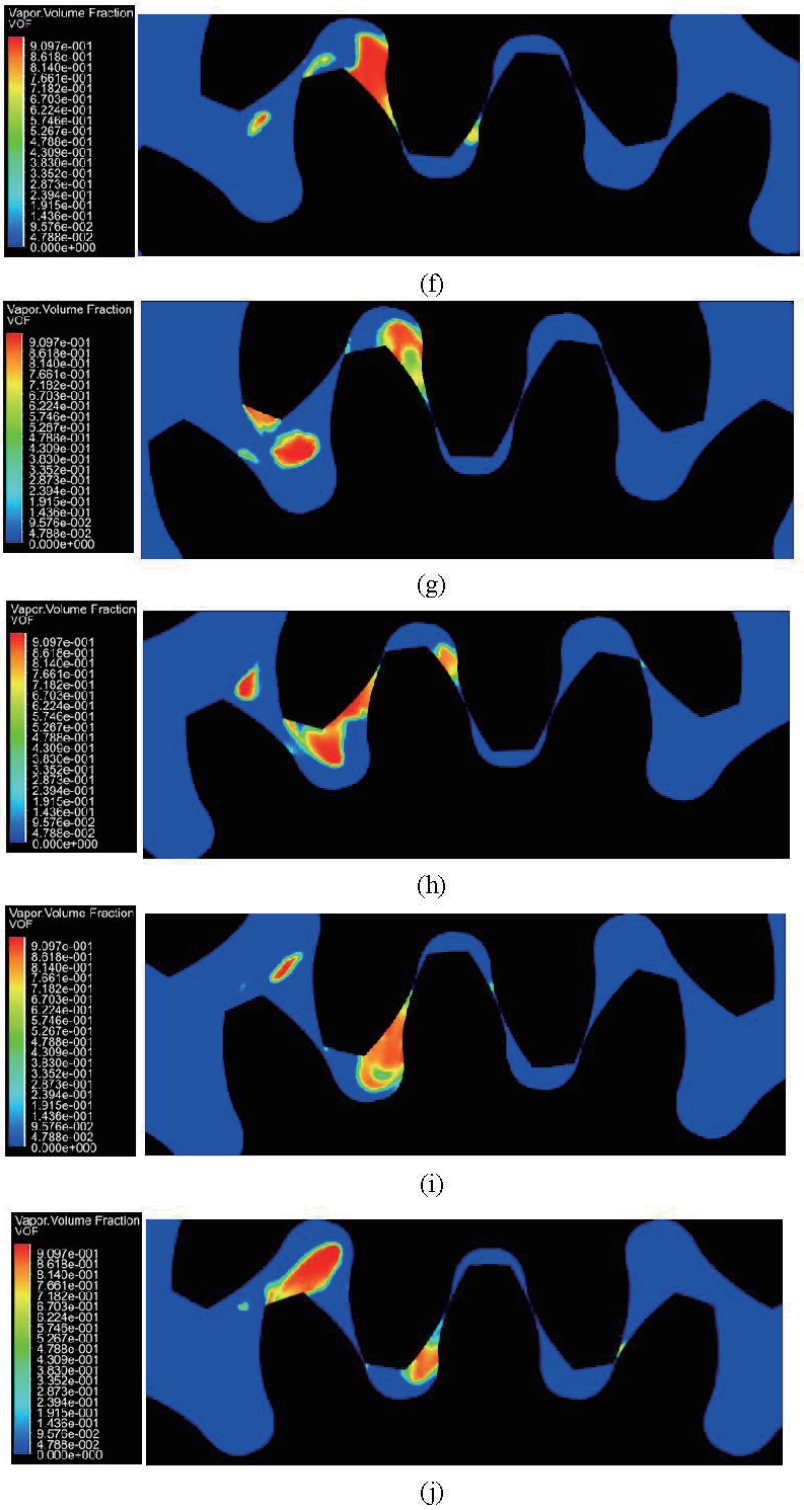

Fig. 17. (Continued) (Color online) Vapor distributions at different times (s): (f) 0.024, (g) 0.028, (h) 0.032, (i) 0.036, and (j) 0.040 s.

Table 2
VoF_{max} values obtained from Fig. 17.

Time (s)	0.004	0.008	0.012	0.016	0.02
VoF_{max}	0.95	0.95	0.96	0.96	0.95
Time (s)	0.024	0.028	0.032	0.036	0.04
VoF_{max}	0.95	0.95	0.96	0.95	0.96

fraction of each fluid in the region. Typical applications include predicting jet rupture, the motion of large bubbles in liquids, the motion of liquids after dam failure, and the steady-state or transient tracking of any gas-liquid interface. Figure 17 shows the contact position of the two gears in Fig. 1 obtained by the VOF method. It can be seen that the entire flow reaches the center position, so the *X*- and *Y*-axes are not shown. The vapor distribution during rotation is shown in Fig. 17, which coincides with the results of other research studies.

4. Conclusion

The flow distribution of a fluid in a gear pump was obtained by model analysis and simulation. The distribution of the fluid was found to be similar to that in previous studies. The mass flow rate and pressure fluctuations during gear rotation were found, and the fluctuation frequency of the gear pump was coupled with that of the gears. Cavitation was observed at locations where the pressure was lower than the saturated vapor pressure. The oil-trapped pressure reached 12.4 MPa. The outlet pressure fluctuated when the oil-trapped pressure was released. This is considered to be the main factor contributing to cavitation. Different gearing conditions have different rates of cavitation. This is because the amount of cavitation decreases with increasing flow rate, which increases the turbulence dynamic energy at saturated vapor pressure. The findings in this study provide basic information on how to develop a system for monitoring and detecting cavitation using sensing technologies.

Acknowledgments

This work was supported by the Research Funding of GDUPT, Research on Heat Transfer Enhancement of Heat Sink by Inverse Calculation Design Method (No. MOST 2019rc074).

References

1 B. R. Munson, A. P. Rothmayer, T. H. Okiishi, and W. W. Huebsch: Fundamentals of Fluid Mechanics (John Wiley & Sons, New York, 2012) p. 24.
2 A. Sou, B. Biçer, and A. Tomiyama: Comput. Fluids **103** (2014) 42. https://doi.org/10.1016/j.compfluid.2014.07.011
3 H. J. Lee, H. Choi, K.-Y. Hwang, D.-C. Park, and S. Min: Int. J. Heat Fluid Flow **68** (2017) 114. https://doi.org/10.1016/j.ijheatfluidflow.2017.10.001
4 Y. Cengel and M. Boles: Thermodynamics: An Engineering Approach (McGraw-Hill, New York, 2015) p. 638.
5 A. S. Ramamurthy and R. Balachandar: J. Fluids Eng. **114** (1992) 439. https://citeseerx.ist.psu.edu/viewdoc/download?doi=10.1.1.822.8033&rep=rep1&type=pdf
6 Y. Inaguma: J. Mech. Eng. Sci. **227** (2013) 980. http://dx.doi.org/10.1177/0954406212456933

7 M. Močilana, Š. Husárb, J. Labajc, and M. Žmindák: Procedia Eng. **177** (2017) 532. https://doi.org/10.1016/j.proeng.2017.02.257
8 H. Shen, Z. Li, L. Qi, and L. Qiao: Mech. Syst. Signal Process. **99** (2018) 921. https://doi.org/10.1016/j.ymssp.2016.09.022
9 S. Li, A. Kahraman, and M. Klein: J. Mech. Design **134** (2012) 041007. https://doi.org/10.1115/DETC2011-47287
10 D. del Campo, R. Castilla, G. A. Raush, P. J. Gamez Montero, and E. Codina: J. Fluids Eng. **134** (2012) 081105. https://doi.org/10.1115/1.4007106
11 A. K. Singhal, M. M. Athavale, H. Li, and Y. Jiang: J. Fluids Eng. **124** (2002) 617. https://doi.org/10.1115/1.1486223
12 Ansys/Fluent 14.5 User's Guide: http://www.pmt.usp.br/academic/martoran/notasmodelosgrad/ANSYS%20Fluent%20Users%20Guide.pdf (accessed March 2022).
13 G. H. Schnerr: Proc. 2001. 4th Int. Conf. Multiphase Flow (ICMFHT, 2001) 1. https://www.researchgate.net/publication/296196752_Physical_and_Numerical_Modeling_of_Unsteady_Cavitation_Dynamics
14 A. G. A. Tomar: J. Electr. Electron. Eng. **4** (2015). https://doi.org/10.4172/2332-0796.1000149
15 H. K. Versteeg and W. Malalasekera: An Introduction to Computational Fluid Dynamics: The Finite Volume Method (Pearson, London, 2007) p. 186.
16 F. J. Kelecy: https://www.semanticscholar.org/paper/Coupling-Momentum-and-Continuity-Increases-CFD/675d6e518d8be3b1b9dda084d2592180d0f1f461 (accessed March 2022).
17 S. V. Patankar: Numerical Heat Transfer and Fluid Flow (Hemisphere, New York, 1980) p. 133.
18 B. P. Leonard: Comp. Methods Appl. Mech. Eng. **19** (1979) 59. https://doi.org/10.1016/0045-7825(79)90034-3
19 M. Keating: https://es.scribd.com/document/337161804/AA-V5-I1-Accelerating-CFD-Solutions (accessed March, 2022).
20 A. Shima, K. Takayama, Y. Tomita, and N. Ohsawa: AIAA J. **21** (1983) 55. https://doi.org/10.2514/3.8027
21 C. Brennen: Cavitation and Bubble Dynamics (Oxford University Press, Oxford, 1995) p. 50.
22 P. J. Zwart, A. G. Gerber, and T. Belamri: Proc. 5th Int. Conf. Multiphase Flow (ICMFHT, 2004). https://www.researchgate.net/publication/306205415_A_two-phase_flow_model_for_predicting_cavitation_dynamics
23 A. P. Keller and H. K. Rott: ASME FED Meeting **4** (1997). https://www.semanticscholar.org/paper/The-effects-of-turbulence-on-cavitation-inception-%C3%8C./35ec97dc75d2befc9bde107d283974056f568520
24 S. Li, A. Kahraman, and M. Klein: J. Mech. Design **134** (2012) 041007. https://doi.org/10.1115/DETC2011-47287
25 D. del Campo, R. Castilla, G. A. Raush, P. J. Gamez-Montero, and E. Codina: J. Fluids Eng. **134** (2012) 081105. https://www.researchgate.net/publication/274768711_Numerical_Analysis_of_External_Gear_Pumps_Including_Cavitation
26 A.Vacca and M. Guidetti: Simul. Model. Pract. Theory **19** (2011) 2007. https://doi.org/10.1016/j.simpat.2011.05.009
27 R. Castilla, P. J. Gamez-Montero, D. del Campo, G. Raush, M. Garcia-Vilchez, and E. Codina: J. Fluids Eng. **137** (2015) 041105. https://doi.org/10.1115/1.4029223
28 H. Kim, H. Marie, and S. Patil: Proc. 2007 American Society of Engineering Education Conf. (ASEE, 2007) 12. https://www.semanticscholar.org/paper/AC-2007-821%3A-TWO-DIMENSIONAL-CFD-ANALYSIS-OF-A-GEAR-Kim-Kim/b7997ac31ff67e69b87648a16819a9bb82a25326
29 S. Chang: Theory and Practice of Hydraulic Machinery (Taipei United Publishing Company, Taipei, 1985) (in Chinese).
30 R. Castilla, P. J. Gamez-Montero, D. del Campo, G. Raush, M. Garcia-Vilchez, and E. Codina: J. Fluids Eng. **137** (2015) 041105. https://doi.org/10.1115/1.4029223
31 J. Stryczek, P. Antoniak, O. Jakhno, D. Kostyuk, A. Kryuchkov, G. Belov, and L. Rodionov: Arch. Civ. Mech. Eng. **15** (2015) 95. https://doi.org/10.1016/j.acme.2014.02.010
32 A. Esposito: Fluid Power with Applications (Prentice-Hall, New Jersey, 1997) p. 158.

About the Authors

Jing-Nan Lin received his B.S. degree from Taipei City University of Science & Technology, Taiwan, in 2004 and his M.S. from National Taipei University of Technology, Taiwan, in 2015. His research interests are combustion, fluid mechanics, noise, and vibration. (bsb690118@gmail.com)

Yu-Ting Tseng received his M.S. degree from National Taipei University of Technology, Taiwan, in 2016. His research interests include fluid mechanics, noise, and vibration. (t106669014@ntut.edu.tw)

Yan-Zuo Chang received his B.S. degree from National Pingtung University of Science and Technology, Taiwan, in 2005, his M.S. degree from National Kaohsiung University of Science and Technology, Taiwan, in 2007, and his Ph.D. degree from National Taipei University of Technology, Taiwan, in 2016. Since 2019, he has been an assistant professor at Guangdong University of Petrochemical Technology, China. His research interests are CFD, bioengineering, and vehicle engineering. (changyanzuo@gmail.com)

Yu-An Chou received his M.S. degree from National Taipei University of Technology, Taiwan, in 2017. His research interests include CFD and vehicle engineering. (t105448024@ntut.edu.tw)

Go-Long Tsai received his B.S., M.S., and Ph.D. degrees from National Tsing Hua University, Taiwan, in 1980, 1982, and 1987, respectively. Since 1995, he has worked as an assistant professor at National Taipei University of Technology, Taiwan. His research interests include CFD, bioengineering, vehicle engineering, and vibration. (golong@gmail.com)

Tian-Syung Lan received his Ph.D. degree from Tatung University, Taiwan, in 2002. His research interests are optimal production control, automation technology, resource integration, and management. (tslan@ydu.edu.tw)